AFRL-RH-WP-TR-2010-0113

Synthetic Observer Approach to Multispectral Sensor Resolution Assessment

Alan R. Pinkus
David W. Dommett
Warfighter Interface Division

H. Lee Task
Task Consulting

Sheldon E. Unger
David W. Sivert
Ball Aerospace & Technologies Corp.

September 2010
Final Report

AIR FORCE RESEARCH LABORATORY
711 HUMAN PERFORMANCE WING,
HUMAN EFFECTIVENESS DIRECTORATE,
WRIGHT-PATTERSON AIR FORCE BASE, OH 45433
AIR FORCE MATERIEL COMMAND
UNITED STATES AIR FORCE

NOTICE AND SIGNATURE PAGE

Using Government drawings, specifications, or other data included in this document for any purpose other than Government procurement does not in any way obligate the U.S. Government. The fact that the Government formulated or supplied the drawings, specifications, or other data does not license the holder or any other person or corporation; or convey any rights or permission to manufacture, use, or sell any patented invention that may relate to them.

This report was cleared for public release by the 88th Air Base Wing Public Affairs Office and is available to the general public, including foreign nationals.

Qualified requestors may obtain copies of this report from the Defense Technical Information Center (DTIC).

AFRL-RH-WP-TR-2010-0113 HAS BEEN REVIEWED AND IS APPROVED FOR PUBLICATION IN ACCORDANCE WITH ASSIGNED DISTRIBUTION STATEMENT.

//signed//
Darrel G. Hopper
Program Manager
Battlespace Visualization Branch

//signed//
Jeffrey L. Craig
Chief, Battlespace Visualization Branch
Warfighter Interface Division

//signed//
Michael A. Stropki
Chief, Warfighter Interface Division
Human Effectiveness Directorate

This report is published in the interest of scientific and technical information exchange, and its publication does not constitute the Government's approval or disapproval of its ideas or findings.

REPORT DOCUMENTATION PAGE

Form Approved
OMB No. 0704-0188

1. REPORT DATE *(DD-MM-YYYY)*	2. REPORT TYPE	3. DATES COVERED *(From - To)*
30-09-2010	Final	Mar 09 – Feb 10

4. TITLE AND SUBTITLE
Synthetic observer approach to multispectral sensor resolution assessment

5a. CONTRACT NUMBER
FA8650-08-D-6801/019

5b. GRANT NUMBER
N/A

5c. PROGRAM ELEMENT NUMBER
63760E

6. AUTHOR(S)
Alan R. Pinkus[*], David W. Dommett[*], H. Lee Task[**], Sheldon E. Unger[***], David W. Sivert[***]

5d. PROJECT NUMBER
DRPA

5e. TASK NUMBER
11

5f. WORK UNIT NUMBER
DRPA11V3 / 71841143

7. PERFORMING ORGANIZATION NAME(S) AND ADDRESS(ES)
Task Consulting[**]
817 S. Bill Martin Dr.
Tucson AZ 85745
Ball Aerospace & Technologies Corp.[***]
2875 Presidential Drive
Fairborn OH 45324

8. PERFORMING ORGANIZATION REPORT NUMBER
N/A

9. SPONSORING/MONITORING AGENCY NAME(S) AND ADDRESS(ES)
Air Force Materiel Command[*]
Air Force Research Laboratory
711th Human Performance Wing
Warfighter Interface Division
Battlespace Visualization Branch
Wright-Patterson AFB OH 45433-7022

10. SPONSOR/MONITOR'S ACRONYM(S)
711 HPW/RHCV

11. SPONSORING/MONITORING AGENCY REPORT NUMBER
711 HPW-RH-WP-TR-2010-0113

12. DISTRIBUTION AVAILABILITY STATEMENT
Approved for public release; distribution is unlimited

13. SUPPLEMENTARY NOTES
88 ABW Cleared 03/05/2010; 88ABW-2010-1007.

14. ABSTRACT Resolution is often provided as one of the key parameters addressing the quality characteristic of a sensor. One traditional approach when determining the resolution of a sensor/display system is to use a resolution target pattern to detect the smallest element that can be "resolved" using the system. This requires a human in the loop to make the assessment. This study investigated the use of a custom designed software approach to generate an effective resolution value for a sensor. Landolt Cs were selected as the resolution target, which were imaged at multiple distances with different sensors. The images were analyzed using custom software to determine the orientation of the C at each distance, which resulted in a probability of correct orientation detection curve as a function of distance. This curve was used to generate a "resolution" for the sensor without involving human vision. Resolution results for four different spectral band sensors were obtained as well as effective resolution of fused images from select pairs of sensors. These results and the possible use of this synthetic observer resolution approach are presented and discussed, as well as possible future research relating this resolution to human visual performance with fused image sources.

15. SUBJECT TERMS: Landolt C, resolution, sensor resolution, image fusion, image quality

16. SECURITY CLASSIFICATION OF:			17. LIMITATION OF ABSTRACT	18. NUMBER OF PAGES	19a. NAME OF RESPONSIBLE PERSON
Unclassified					Darrel G. Hopper
a. REPORT	b. ABSTRACT	c. THIS PAGE			19b. TELEPHONE NUMBER (*Include area code*)
UNCL	UNCL	UNCL	SAR	22	937-255-8822

Standard Form 298 (Rev. 8-98)
Prescribed by ANSI-Std Z39-18

THIS PAGE INTENTIONALLY LEFT BLANK

TABLE OF CONTENTS

LIST OF FIGURES

LIST OF TABLES

GLOSSARY

ALCOR	Auto-Landolt C Orientation Recognition
BMP	bit map picture
FG	frame grabber
LWIR	long wave infrared
MTF	modulation transfer function
MRAD	milliradian
NIR	near infrared
QED	Quad Emissive Display
SVGA	super video graphics display
SWIR	short wave infrared
VGA	video graphics display
VIS	visible

1.0 SUMMARY

Resolution is often provided as one of the key parameters addressing the quality characteristic of a sensor. One traditional approach when determining the resolution of a sensor/display system is to use a resolution target pattern to detect the smallest element that can be "resolved" using the system. This requires a human in the loop to make the assessment. This study investigated the use of a custom designed software approach to generate an effective resolution value for a sensor. Landolt Cs were selected as the resolution target, which were imaged at multiple distances with different sensors. The images were analyzed using custom software to determine the orientation of the C at each distance, which resulted in a probability of correct orientation detection curve as a function of distance. This curve was used to generate a "resolution" for the sensor without involving human vision. Resolution results for four different spectral band sensors were obtained as well as effective resolution of fused images from select pairs of sensors. These results and the possible use of this synthetic observer resolution approach are presented and discussed, as well as possible future research relating this resolution to human visual performance with fused image sources.

2.0 INTRODUCTION

2.1 Resolution measurement background and philosophy

Over the years, there have been many methods developed to determine the image quality of an image-generating system such as a sensor/display combination[1]. In most cases, the final consumer of the image produced is a human observer using their visual capability to extract visual information from the displayed image. In recent years, imaging systems and image manipulation have moved from the analog world to the digital world, which has probably added a bit more confusion to the issue of image quality or resolution. In general, resolution is the ability of a sensor/display system to produce detail; the higher the resolution the finer the detail that can be displayed. With the advent of digital imagery and sensor detectors that are composed of an array of discrete elements, it is tempting, and not entirely wrong, to characterize the resolution of the system by the number of picture elements (pixels) for the display or sensor elements in the case of the sensor. For example, VGA resolution for computer displays is 480 elements high by 640 elements wide and SVGA is 600×800 elements. This describes the number of samples that can be displayed but it says nothing of the quality of the actual display medium characteristics (luminance, contrast capability, noise, color, refresh rate, active area to total area ratio, etc.) or of the signal/information used to feed the individual pixels. Nevertheless, this numerical value of pixel or sensor element count is often given as a primary metric for the resolution (quality) of the sensor or display.

Another common approach to determining the resolution of a sensor/display system is to image an appropriate resolution test target and determine the smallest sized critical test pattern element that can be seen by a human observer[2,3,4,5]. Many test patterns have been developed over the years such as gratings, tri-bars, tumbling Es, the Snellen chart, and the Landolt C chart to test vision or to test imaging systems using vision[6]. The test pattern typically has test elements of various sizes so that the human observer can pick out the smallest size that they can resolve. In this case, one needs to make sure that the resulting test image size on the display is well within

human vision capability so that what is really being tested is the imaging system and not the visual system of the observer. An alternative to the multi-sized test pattern is to use a single size test element but image it at various distances until a distance is obtained at which the test object is barely resolved.

For this effort, we selected the Landolt C as the resolution target and we used distance from the sensor to the target as the method for probing the resolution of the sensor. We also selected four sensors representing four different spectral bands for resolution measurement. The following section provides the details of the approach to making semi-automated resolution measurements of sensors and fused images produced from pairs of sensors.

3.0 APPROACH

As noted above, our basic approach was to obtain images of a Landolt C resolution target at different distances and feed these images into a custom software algorithm to see how well the software could correctly determine the orientation of the C as a function of distance. From these data we could then calculate a "resolution" from the sigmoid curve fit to these data. Using this approach it is possible to determine the resolution for multispectral fused images (a synthetic sensor) and later, compare resolutions determined by the software to resolutions determined from human testing. The following sections describe this approach in more detail.

3.1 Sensors and zoom lane

Table 1 is a summary of the four sensors that were selected for this study along with their basic characteristics. The four spectral bands selected were long-wave infrared (LWIR), short-wave infrared (SWIR), near infrared (NIR) and visible (VIS). The basic number of sensor elements is listed in column 4 of Table 1 along with the measured horizontal field of view (column 5) and the calculated individual sensor element "resolution," which was determined by dividing the horizontal field of view by the number of horizontal sensor elements (and then converting the results to milliradians). The calculated sensor "resolution" (last column in Table 1) is a reasonable estimate of the level of detail that the sensor should be able to detect. It is this column of "resolution" numbers that will be compared with the sensor resolutions obtained by the Landolt C test procedure used in this study. Figure 1 shows the sensor suite[7] with the sensors mounted as close together as physically possible to minimize registration problems with the fused images. Figure 2 shows the sensor suite mounted to a computer-controlled, movable cart mounted on a track that can be positioned at selected distances from the resolution target pattern at the end of the zoom lane.

Table 1. The four sensors used in this study and their relevant characteristics

Manufacturer	Sensor	Spectral Band	Array Size (H×V)	Measured Horizontal FOV (deg)	Calculated Resolution for Horizontal (mrad)
BAE	LTC550	LWIR (7-15μm)	320×240	35.9	1.96
Sensors Unlimited	SU320	SWIR (0.9-2.5 μm)	320×240	30.7	1.67
ITT	ISA-780	NIR (0.665-0.9 μm)	768×493	31.2	0.71
Sony	XC-73	VIS (0.4-0.75 μm)	768×494	33.2	0.75

Figure 1. Multispectral suite of four sensors

Figure 2. Sensor suite mounted on a movable cart

3.2 Resolution target pattern and the sensor image collection procedure

The test pattern was a 62.5mm high/wide Landolt C (gap size of 12.5mm) that was mounted to a device designed to provide reasonable spectral energy across all four spectral bands of the sensors selected. This device, dubbed the quad-emissive display (QED), is more fully described in Pinkus and Task (2009)[7]. Figures 3 and 4 show the QED with the Landolt C mounted in place. The front surface is illuminated with incandescent light appropriate to the sensor(s) being used and the rear plate is heated to provide an accurately controlled temperature difference between the plastic, white front surface and the flat black, metallic back surface. The Landolt C is actually a stencil, or cut-out, so that the black back surface shows through the stencil opening. The Landolt C can be mounted in any of the four cardinal positions (gap pointing up, right, down, or left).

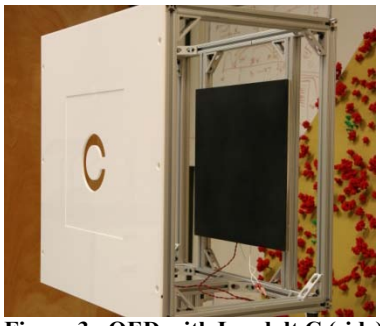

Figure 3. QED with Landolt C (side)

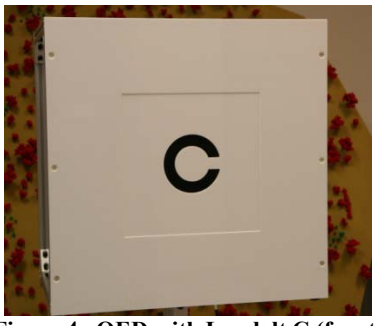

Figure 4. QED with Landolt C (front)

The basic procedure was to position the movable cart, with the four sensors mounted to it, at a specific distance and then capture images from all four sensors at the same distance. This was done with the Landolt C oriented in each of the four cardinal directions. However, preliminary testing resulted in two modifications to this basic procedure.

First, the set of distances used for the "higher resolution" sensors (the VIS at 0.75 mrad and the NIR at 0.71 mrad) were different (farther away) than those used for the "lower resolution" sensors (the LWIR at 1.96 mrad and the SWIR at 1.67 mrad). Table 2 is a summary of the distances used to collect images for each of the sensors along with the calculated resolution based on the field of view and sensor horizontal element count. This was done to minimize the number of images that needed to be recorded for each sensor. It was expected that the measured

resolution of each sensor, discussed more fully below, would be in the general range of the previously discussed calculated resolution. Based on the fundamental concept of resolution for the Landolt C, one would expect the distance at which the gap in the Landolt C could be "resolved" is the distance at which the angular subtense of the gap is approximately equal to the calculated resolution of the sensor. The first row of Table 2 lists the calculated resolutions for each of the sensors, which can be compared with the corresponding angular subtense of the gap size for each image collection distance. Selecting different collection distances for the different sensors reduced the overall number of images required but, it also made it impossible to look at certain fused image combinations, such as VIS with LWIR, since there were insufficient images taken at the same distance with the same sensor.

Second, it was determined that there was a sampling issue with respect to the relative position of the Landolt C gap and the individual sensor elements. Depending on where the Landolt C gap fell with respect to the sensor element, the C might be more or less interpretable. This phenomenon would presumably have similar effects on either a human observer or a software algorithm intended to mimic an observer's visual performance with these images. In order to at least partially offset the effect just described, it was decided to capture images of the Landolt C at multiple lateral and vertical "shifts" so there would be a rather large collection of relative C-gap/sensor element positions. This was implemented by moving the QED target pattern $1/5^{th}$ of the gap size (2.5mm) in both vertical and horizontal directions resulting in a 5×5 matrix of images of the Landolt C for each orientation at each distance. Therefore, there were 100 images captured for each sensor at each distance (five lateral shifts times five vertical shifts times four orientations).

Table 2. Summary of distances used for each sensor

Sensor-calculated Resolution			Sensor-calculated Resolution		
1.96 mrad	1.67 mrad		0.71 mrad	0.75 mrad	
LWIR	SWIR	C-gap Size	NIR	VIS	C-gap Size
(meters)	(meters)	(mrad)	(meters)	(meters)	(mrad)
6	6	2.08	10	10	1.25
7.5	7.5	1.67	13	13	0.96
9	9	1.39	16	16	0.78
11	11	1.14	20	20	0.63
13	13	0.96	24	24	0.52
16	16	0.78	28	28	0.45
	19	0.66	34	34	0.37

Each of the four sensors provided an analog signal output (RS-170) that was fed into a frame grabber to capture a single frame of the output. The frame grabber converted the signal into a single frame with 640 horizontal by 480 vertical elements. Since two of the sensors (VIS and NIR) had somewhat greater sensor element counts (768×494) than this matrix, it is probable that the frame grabber limited the measurement of resolution for these sensors. While this is not a desirable situation, it does not detract from the main objective of this project, which is to devise a software algorithm that will produce similar resolution assessment results as a panel of human observers. Since the images "viewed" by both the software algorithm and the human observers

are the same, the fact that the VIS and NIR sensor resolutions might be measured as somewhat poorer than what they really are (due to the frame-grabber limitation) does not take away from the human observer/software algorithm comparison. However, in order to seriously use this technique to determine sensor resolution, one needs a frame grabber with an element count comfortably in excess of any sensor being tested. All images captured by the frame grabber were saved in BMP format for analysis by the software algorithm.

3.3 Sensor resolution determination

The software developed to determine the C's orientation has been named ALCOR which stands for Auto-Landolt C Orientation Recognition. The ALCOR software needed to do two basic things: 1) find the Landolt C in the image and 2) determine the orientation of the Landolt C. Of these two, determining the orientation of the Landolt C was deemed to be, by far, the most important since it is this function that is used to determine the resolution of the sensor. However, this function could not be achieved until after the Landolt C position was identified in the software. To facilitate the location of the Landolt C, the QED target pattern generator was positioned so that it would be approximately in the center of each of the images captured from the sensors. The QED target pattern generator had a fairly uniform surround around the Landolt C stencil (see Figures 3 and 4) to aid in picking out the Landolt C from its immediate surround. The central 100×100 pixels were searched to find the center of the Landolt C. Once the center of the Landolt C was identified, the collection of pixels in the up, down, left, and right directions were analyzed to determine the direction that had a high likelihood of containing the Landolt C gap. Since the Landolt C target was always a dark (low signal level) C on a light (high signal level) background, the gap should be in the direction of the highest signal level (the direction that does not cross over the lower signal level C). This is somewhat analogous to a radar display sweep checking the four cardinal directions for which direction has the highest "return."

Once the software determined the probable direction of the Landolt C, the software would compare this direction to the correct direction (which was coded into the image file name along with the sensor type and the distance from which it was recorded). The software then provided two outputs. One was a summary report of all of the images in the file showing the number of correct determinations of orientation for each distance and the other was a graphic of the central set of pixels of each image. This graphic had the direction vector marked in green if the software-determined direction was correct or in red if the software was wrong (with a blue vector indicating the correct direction). Samples of these outputs are shown in Figures 5 and 6 for a relatively close distance (all responses were correct) and a farther distance (one of the responses was wrong) respectively.

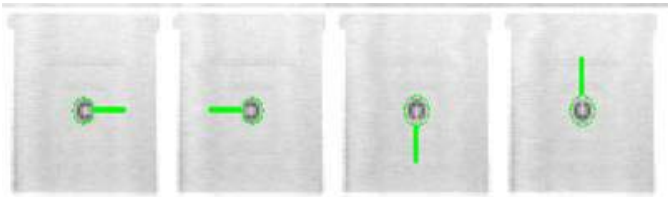

Figure 5. Graphic output from the ALCOR software showing that it determined the Landolt C direction correctly

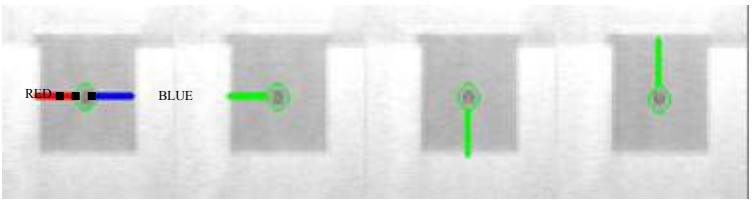

Figure 6. Example of graphic output of the ALCOR software in which it got the first orientation wrong (it guessed the red-dashed line direction to the left but the correct orientation was the blue line direction to the right)

Although the ALCOR software is capable of looking for the Landolt C orientation in eight directions (up, down, left, right and upper-left, upper-right, lower-left, lower-right), it was limited to just the four orientations for this study.

After all of the images at the different distances were assessed by the ALCOR software, the percent correct was graphed against the distance for each sensor. To determine a resolution value from these data, it was necessary to fit a curve to the data. Logistic regression[8] was selected as the method of curve-fitting. The form of the generalized logistic equation used for this effort is shown below.

$$Logit_i = \ln\left(\frac{p-k}{1-p}\right) = B_1 * X_i + B_0 \quad (1)$$

where:

p = probability of occurrence (in our case, the probability of correct C orientation determination)

k = constant (in this case, 0.25, which is the probability of guessing the correct orientation of the C)

B_1 = slope determined by the linear regression of the logit with distance

B_0 = intercept determined by the linear regression of the logit with distance

X_i = distance from sensor to Landolt C target

$Logit_i$ = the percent correct at distance X_i (for this case).

The values of B_0 and B_1 were determined for each sensor by performing a linear regression (least squares fit) of the percent correct versus distance. Since we are primarily interested in the probability of correct determination of the Landolt C orientation as a function of distance, Equation 1 needs to be solved for p. Equation 2 is the resulting equation that is graphed as the best fit curve for the data collected.

$$p = \frac{1-k}{1+e^{-(B_0+B_1*d)}} + k \quad (2)$$

where:

p = probability of obtaining the correct orientation of the Landolt C

k = baseline probability (1 chance in 4 of getting the correct orientation by guessing, i.e., 0.25)

B_1 = slope determined by the linear regression of the logit with distance

B_0 = intercept determined by the linear regression of the logit with distance

d = distance from sensor to Landolt C target.

The next step in determining a resolution value for each sensor is to select a criterion point. It was decided to select a distance value that corresponded to a point on the logistic fit curve that was half way between chance (0.25) and 100% correct (1.00). This is somewhat similar to a 50% probability threshold curve where the software is correct (after subtracting the 25% for chance) about half of the time. The probability value that corresponds to this resolution distance is half way between 0.25 and 1.00 or (1.00 + 0.25)/2 = 0.625. Referring back to Equation 1 we see that when we substitute the values of k = 0.25 and p = 0.625 into the equation we get,

$$Logit = \ln\left(\frac{p-k}{1-p}\right) = \ln\left(\frac{0.625-0.25}{1-0.625}\right) = \ln\left(\frac{0.375}{0.375}\right) = \ln(1) = 0. \quad (3)$$

This means the resolution distance is that distance for which the linear best-fit curve expression at the right side of Equation 1 equals zero. In equation form,

$$\ln\left(\frac{p-k}{1-p}\right) = 0 = B_1 * d_R + B_0, \quad (4)$$

which can easily be solved for d_R, the resolution distance (Equation 5 below).

$$d_R = -\frac{B_0}{B_1} \quad (5)$$

where:

d_R = resolution distance
B_0 = intercept of the linear regression equation
B_1 = slope of the linear regression equation.

The resolution distance for the sensor is the distance at which the Landolt C can be correctly interpreted at a rate half way between chance (25%) and certainty (100%). The measured sensor resolution is then the angular subtense of the Landolt C gap size (12.5mm) at this distance, which is given by Equation 6.

$$\text{Measured Sensor Resolution} = R_m = (12.5/d_R) \text{ in milliradians} \quad (6)$$

where:

R_m = measured resolution in milliradians
d_R = resolution distance in meters.

One problem with using Equation 1 for curve fitting is that the logit is undefined for any data point that is equal to or below 0.25. Luckily, for our data set (Tables 3 and 5), all fraction correct values were in excess of the 0.25 chance level. If this had not been the case we would have had to substitute 0.25 for any percent correct data point that was below 0.25. The logit is also not defined for a fraction correct value of 1.00 so a value of 0.999 was entered.

3.4 Sensor noise issue

Of the four sensors selected, it was apparent that the NIR sensor, basically the same spectral sensitivity as night vision goggles, had the most noise at the illuminance levels used. The human visual system can "average out" this noise to some degree. Therefore, it was decided to collect and

average 10 consecutive video frames from the NIR sensor to simulate, to some extent, the human's visual capability for each image that was used for assessing the NIR sensor resolution.

3.5 Synthetic sensor (fused images) resolution

Once all of the images from all sensors and all distances were collected, it was possible to register and fuse images collected from different sensors for the same distances. Since the fields of view of the sensors varied somewhat, images did have to be resized in order to register and fuse the images. Two "synthetic" sensors were evaluated in this fashion: the combination of the VIS and NIR sensors and the combination of the SWIR and LWIR sensors. It should be remembered that for this project, the Landolt C target always had the same contrast parity; that is, it was always a dark C on a light background for all sensors making it somewhat easier to fuse the two images.

4.0 RESULTS

4.1 Basic sensor results

Table 3 is a summary of the fraction correct responses from the ALCOR software for the four sensors at the various distances used. As can be seen from this table, the fraction correct is very high for the shorter distances for each sensor and then drops off to close to chance only (25% correct) at the farthest distances. Figure 7 shows graphs of the data shown in Table 3 along with the best-fit logit regression curves. Table 4 is a summary of the calculated resolution for each sensor (based on number of horizontal elements and the horizontal field of view) compared with the sensor logit curve fit value at 62.5 percent probability of correct response. The last column of Table 4 is the ratio between the resolution measured using the logit fit curve and the calculated resolution.

Table 3. Fraction correct Landolt C orientation determination as a function of distance for each sensor. The column labeled "C-gap Size" is the angular subtense of the Landolt C at the distances shown; these can be compared to the sensor-calculated resolution

Sensor-calculated Resolution	1.96 mrad	1.67 mrad	C-gap Size (mrad)
Distance (meters)	LWIR	SWIR	
6	0.99	0.98	2.08
7.5	0.92	0.99	1.67
9	0.77	0.99	1.39
11	0.67	0.98	1.14
13	0.56	0.67	0.96
16	0.29	0.63	0.78
19		0.26	0.66

Sensor-calculated Resolution	0.71 mrad	0.75 mrad	C-gap Size (mrad)
Distance (meters)	NIR	VIS	
10	1.00	0.97	1.25
13	0.92	0.98	0.96
16	0.87	0.87	0.78
20	0.58	0.79	0.63
24	0.39	0.63	0.52
28	0.36	0.40	0.45
34	0.26	0.30	0.37

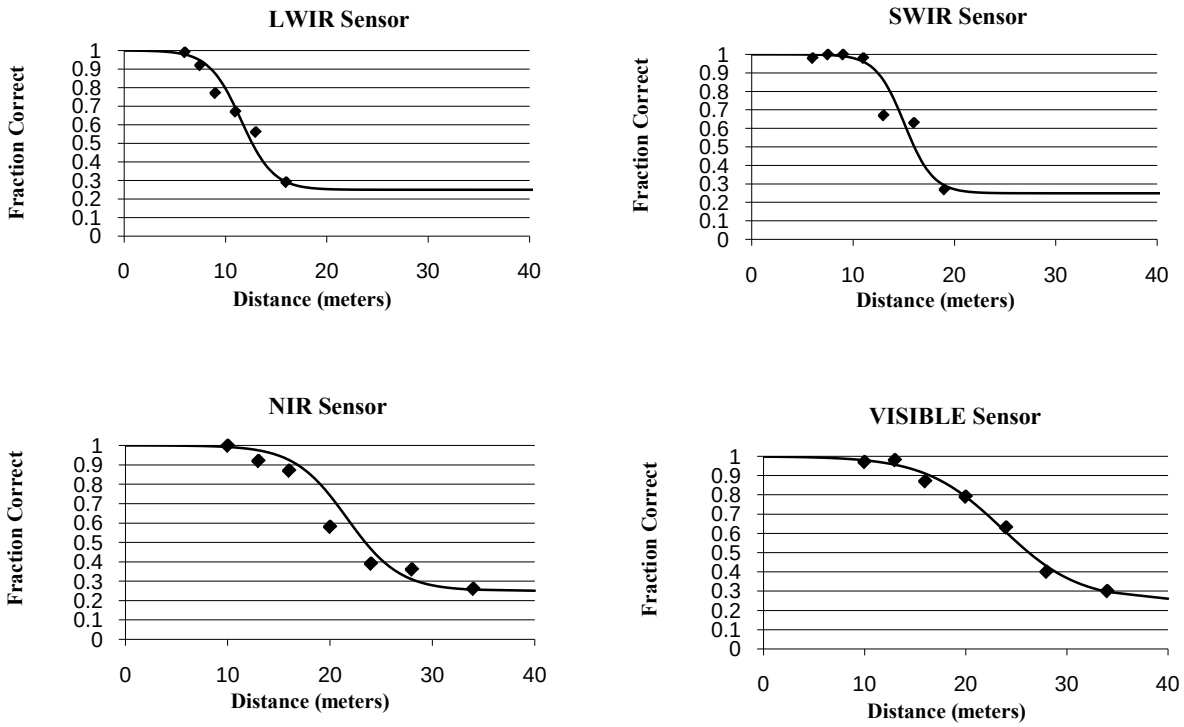

Figure 7. Graphs of the fraction correct responses for each of the four sensors as a function of distance with logistic regression curve

Table 4. Comparison of the calculated and measured resolutions (milliradians or mrad) and the ratio between the two

Sensor	Calculated Resolution (mrad)	Measured Resolution (mrad)	Ratio
SWIR	1.67	0.83	0.50
LWIR	1.96	1.08	0.55
VIS	0.75	0.53	0.71
NIR	0.71	0.58	0.81

4.2 Fused "sensor" results

Table 5 is a summary of the fraction correct Landolt C orientation determination as a function of distance for two sensor combinations: the SWIR-LWIR and the VIS-NIR. These were the only two combinations that could be tested because of the aforementioned issue with images being collected at different distances for the "low resolution" and "high resolution" sensors. The images from the pairs of sensors were fused in two different ways: using a simple averaging algorithm and using a LaPlacian algorithm. Figure 8 shows graphs of the SWIR-LWIR fused data of Table 5.

Table 5. Summary of percent correct as a function of distance for the fused sensor image combinations shown

SWIR-LWIR Fused		
Distance (m)	LaPlacian	Average
6	0.73	0.8
7.5	0.85	0.95
9	0.89	0.98
11	0.69	0.68
13	0.48	0.49
16	0.32	0.33

VIS-NIR Fused		
Distance (m)	LaPlacian	Average
10	0.96	0.93
13	0.99	0.81
16	0.79	0.79
20	0.55	0.61
24	0.4	0.49
28	0.26	0.26
34	0.29	0.35

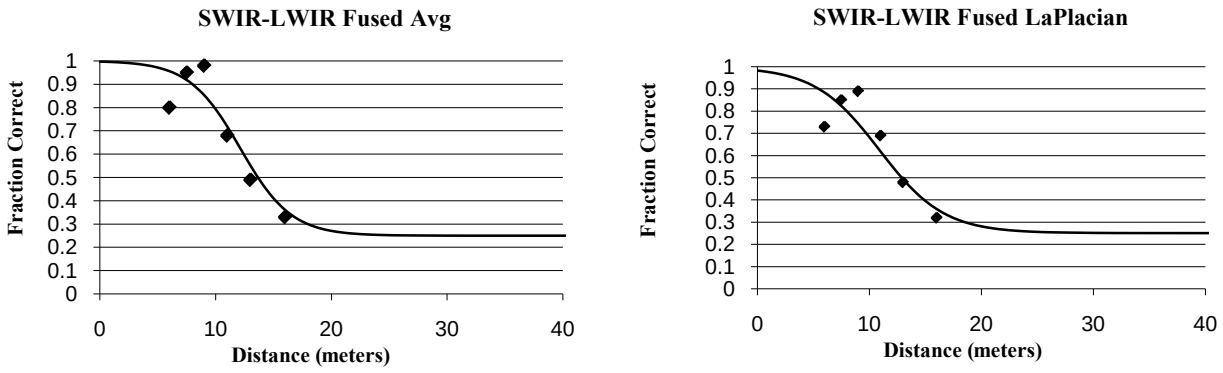

Figure 8. Graphs of the SWIR-LWIR fused image data from Table 5 with Averaging and LaPlacian fusion algorithms

It is apparent from the graphs of Figure 8 that the fraction correct data are dropping at the lowest two distances, which is not intuitive. Inspection of these images indicates that they are easily interpretable to human vision. This low-end roll-off only occurred with the "low resolution" sensor fusion and is slightly evident when looking at the SWIR sensor curve as well. We are not sure why this effect occurred but it is obviously a quirk of the ALCOR software that needs to be addressed in the future. In order to provide a reasonable assessment of the measured resolution, it was decided to apply the logistic regression curve fit with the two lowest distances deleted for the SWIR-LWIR fusion combinations. This only has a small impact on the measured resolution (as shown in the table below) but it provides a much more pleasing curve fit as indicated in the graphs of Figure 9. These two modified curve-fits are designated SWIR-LWIR fused Average B and SWIR-LWIR fused LaPlacian B to differentiate them from the curve fits that use all of the data points.

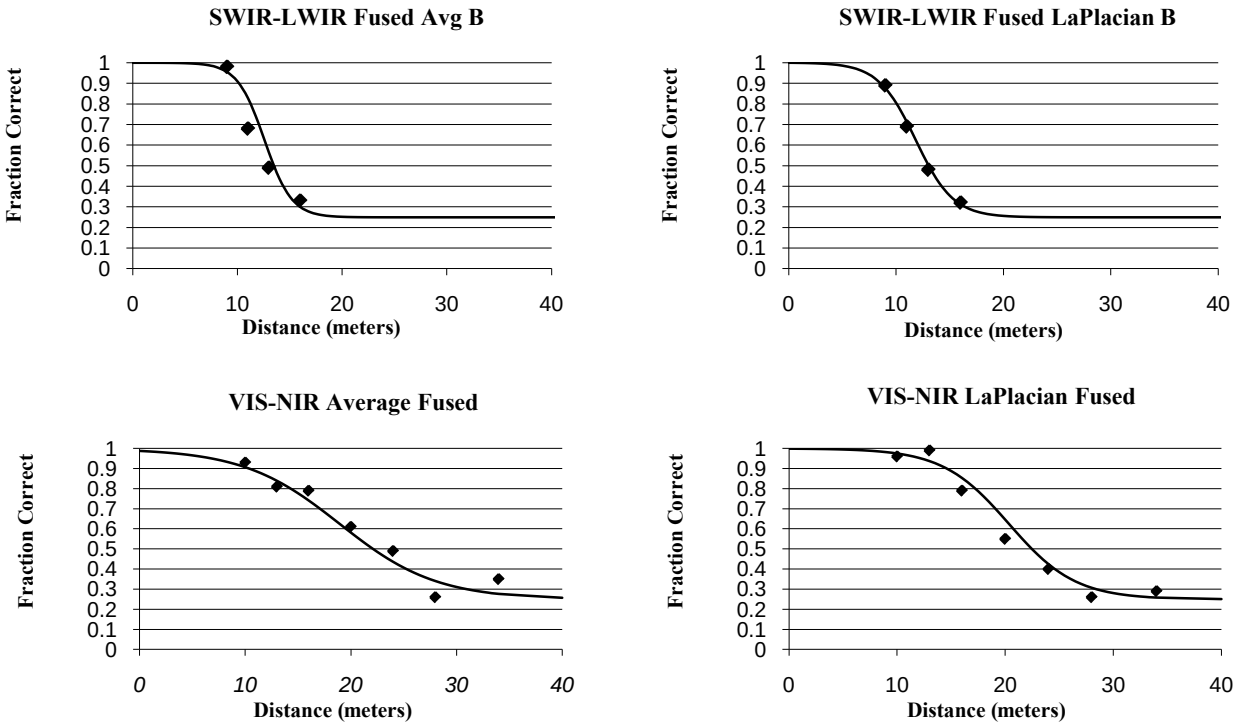

Figure 9. Fused image curves using data from Table 5

Table 6. Summary of measured resolutions for the fused sensor combinations; the smaller the number the better the resolution

Fused Sensor Combinations	Resolution (mrad)
SWIR	0.83
LWIR	1.08
SWIR-LWIR LaPlacian	1.15
SWIR-LWIR Average	1.03
SWIR-LWIR LaPlacian B	1.06
SWIR-LWIR Average B	0.99

Fused Sensor Combinations	Resolution (mrad)
VIS	0.53
NIR	0.58
VIS-NIR LaPlacian	0.61
VIS-NIR Average	0.66

5.0 ANALYSIS

5.1 Comparison of calculated resolution and measured resolution

Previously it was noted that the sensor element count for the VIS and NIR sensors exceeded the frame-grabber element count, which would impact the value of the calculated resolution (field of view/sensor element count). One way to, at least partially, correct for this is to substitute the frame-grabber element count for the sensor element count to obtain a modified calculated resolution. Table 7 below shows these modified calculated resolutions for the VIS and NIR sensors, which are

designated VIS FG and NIR FG with the "FG" signifying the frame-grabber element count was used in the calculation.

Table 7. Same as Table 4 except with modified calculated resolutions for the VIS and NIR sensors to account for the limiting effects of the frame-grabber (FG) element count

Sensor	Calculated Resolution (mrad)	Measured Resolution (mrad)	Ratio
SWIR	1.67	0.83	0.50
LWIR	1.96	1.08	0.55
VIS FG	0.90	0.53	0.59
NIR FG	0.85	0.58	0.68

Using the calculated resolutions of Table 7, it is possible to do a linear regression to determine how well the calculated resolution can predict the measured resolution obtained using the ALCOR software and logit regression. Figure 10 is a graph of the data of Table 7 with the linear best-fit line shown. The correlation between the calculated resolution (with the frame-grabber limitation modification) and the measured resolution was 0.97. This indicates the calculated resolution does a fairly good job of predicting the measured resolution, although the values are not close (the measured resolution is about 50% to 68% of the calculated resolution as indicated by the "Ratio" column of Table 7).

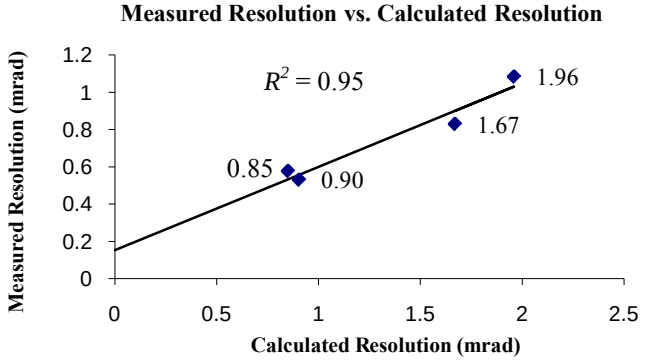

Figure 10. Measured resolution versus calculated resolution using the data from Table 7; correlation is 0.97

Based on this analysis, it appears that the measured resolution is reasonably consistent with the calculated resolution for the sensors and the range of resolutions involved.

5.2 Measured resolution of "synthetic" sensors

The next question is: What do the measured resolutions of the "synthetic" sensors (the fused combinations of sensors) look like compared to the measured resolutions of the component sensors? The data for this comparison are in Table 6, which is discussed in the next section.

6.0 DISCUSSION/CONCLUSIONS

6.1 Comparison of calculated resolution versus measured resolution

Although it was not a primary purpose of this study, the relationship between the sensor resolution measured using the ALCOR software approach and the sensor resolution calculated from the sensor pixel count and field of view is of interest. The measured resolution includes any effects that may be present that could affect the image quality of the sensor such as the lens modulation transfer function (MTF), sensor element noise, and optical defocus whereas the calculated resolution is not sensitive to these (and other) potential defects. However, assuming these potential defects do not have a substantial impact on the actual resolution of the sensors we selected for our study we would expect there to be a reasonable correlational relationship between the two resolutions. Table 7 and Figure 10 demonstrate there is a fairly strong relationship between the two (R-squared value of 0.95), which is encouraging. Ideally, one would like to see a correlation of 1.00 and an intercept of 0 for the linear regression line between the two resolutions. We obtained a correlation of 0.97 (close to 1.00) but an intercept of 0.15 mrad (larger than desired), indicating that there were probably some non-geometric (pixel spacing and lens focal length) parameters affecting the image quality. From Table 7 one can see that the NIR sensor had a better calculated resolution (based on geometry) than the VIS sensor but the VIS sensor had a better measured resolution (ALCOR) than the NIR sensor. Based on visual inspection of the images, this is almost certainly due to the noise in the NIR sensor images even though they were averaged across 10 frames.

6.2 Measured resolution of "synthetic" sensors

Table 6, showing the results of the measured resolution (ALCOR) for the different fused sensor combinations and fusion algorithms, is the basis for this discussion. As can be seen in Table 6 both of the fusion algorithms (Average and LaPlacian) for the high-resolution sensor combinations (VIS and NIR) had poorer measured resolutions (higher numbers) than either of the component sensor measured resolutions. This is most likely due to the problem of having to register the images from the two sensors prior to fusion. The fused resolutions of these two sensors ranged from 6% to 25% worse than the component sensor resolutions depending on which fusion algorithm and which base sensor one is comparing to. Based on this result, one would expect the fused images of this sensor combination to have a lower resolution than either component sensor by itself but this does not necessarily mean that human visual performance for an actual, field-relevant task (such as target detection or target recognition) would be worse with the fused images. Human visual performance depends not only on the resolution of the fused images but also on the scene-specific image content. The information content of the fused images depends largely on the scene characteristics and it may be that this visual information content difference between the two component sensors could be more significant than the loss of resolution due to image registration/fusion. This is an area worthy of further study.

The results for the SWIR-LWIR "synthetic" sensor were somewhat different. For this case, the fused sensor resolution ranged from an improvement in resolution of about 8% to a decrement of about 28% depending on which baseline sensor is being compared to which fusion algorithm. The major difference between this sensor combination and the "high resolution" sensors combination is the difference in measured resolution between the two sensors that are fused. The difference in resolution between the SWIR and the LWIR sensors was about 27% whereas the difference in

resolution between the VIS and NIR sensors was only about 9%. This might help explain the "improvement" effect found with respect to the LWIR sensor compared to the SWIR-LWIR fusion. Namely, that the SWIR sensor resolution (higher resolution) had enough of an impact on the SWIR-LWIR fusion algorithms that it "over-powered" resolution losses from the registration process when compared to the LWIR sensor resolution.

For the SWIR-LWIR "synthetic" sensor, the Average fusion algorithm was about 6% better than the LaPlacian fusion algorithm but for the VIS-NIR "synthetic" sensor, the LaPlacian was about 8% better than the Average. Given that we do not know the level of repeatability of the ALCOR software resolution measurement procedure and the small percentages noted here, there is no clearly apparent advantage to either the Averaging algorithm or the LaPlacian algorithm.
Overall, it appears that the resolution (as measured by the ALCOR software approach) of the "synthetic" sensors is generally worse (larger number) when compared to the resolution of the component sensors, probably due to the registration process.

6.3 Future research – comparison of ALCOR resolution with human visual resolution assessment

The work described in this paper is the first half of a two-part program to compare sensor resolution assessment accomplished using a novel software algorithm approach (ALCOR) with sensor resolution assessment accomplished using a panel of human observers. The research protocol and review by the human use review committee to conduct the human panel research has been completed and, by the time this paper is published, should be in process. All of the measured sensor resolutions addressed in this paper will be measured in a similar fashion (logistic regression curve fit value at 62.5% probability) but with a panel of human observers viewing the images to determine the orientation of the Landolt C to obtain the fraction correct data. These data will then be compared to see if the ALCOR software approach provides similar results to the human panel approach.

Assuming the results of the future research described immediately above is successful, then another interesting study would be to include the resolution target (the Landolt C in our case) within sensor images that contain operationally relevant targets. These images could then be used in simultaneous efforts to determine their resolution using the ALCOR software methodology and human visual performance (probably target recognition) using the operationally relevant targets within the same images. This could be done for both the individual sensors and the "synthetic" sensors to see if resolution values can predict human visual performance levels.

Another area for future research is to conduct the same ALCOR software-based resolution assessment procedures on sensors that have highly mismatched resolutions due to significant differences in sensor element counts.

For the current effort, we used a 5×5 matrix of resolution target "shifts" in order to average out potential sampling issues with respect to the relative position of individual sensor elements and the Landolt C gap. It would speed up the process if we could get the same results using a 3×3 matrix of image shifts to cut down the number of images at each distance from 100 (5×5 shifts by 4 orientations) to 36 (3×3 shifts by 4 orientations).

The ultimate goal of this line of research is to devise an objective technique to reliably predict fusion algorithm effectiveness without having to conduct human-based visual performance studies.

6.4 Conclusions

The research conducted so far has resulted in a software algorithm (ALCOR) that produces an objective measure of sensor resolution including "synthetic" sensors that are produced by fusing the images from different sensors that have different spectral band sensitivities.

The correlation between simple geometrically based sensor resolution calculations and the sensor resolutions measured using the ALCOR software algorithm and logit regression was quite good ($R^2 = 0.95$). This helps validate the basic approach of the ALCOR software. However, there is no geometrically based sensor resolution for "synthetic" sensors since component sensors used to produce the fused images may have different basic resolution geometries (sensor element spacing and lens focal length). The ALCOR approach potentially provides a means of determining the resolution of a non-existent, "synthetic" sensor. Future work will have to address the repeatability of the ALCOR approach.

Based on our limited sample size (four sensors and four "synthetic," fused sensors), it appears that, in general, synthetic sensors have poorer resolutions than their component sensor resolutions which is probably due to the registration process. This is another area for future work.

7.0 REFERENCES

[1] Task, H. L., "An evaluation and comparison of several measures of image quality of television displays," Report No. AMRL-TR-79-7 DTIC No. A069690 Wright-Patterson AFB OH Aerospace Medical Research Laboratory, (1979).

[2] Task, H. L. and Pinkus, A. R., "Theoretical and Applied aspects of night vision goggle resolution and visual acuity assessment," Proc. SPIE 6557, 65570P-1-11 (2007).

[3] Pinkus, Alan R., Task, H. L., Dixon, Sharon and Goodyear, Chuck, **"**Reproducibility limits of night vision goggle visual acuity measurements," SAFE Journal 30(1), 131-139 (2000).

[4] Pinkus, A. R., and Task, H. L., "Measuring observers' visual acuity through night vision goggles," SAFE Symposium Proceedings 1998 36th Annual Symposium, 1-11 (1998).

[5] NATO STANAG 4349, "Measurement of the minimum resolvable temperature difference (MRTD) of thermal cameras," (1995).

[6] Farrell, R. J., and Booth J. M., Design handbook for imagery interpretation equipment, Boeing Aerospace Co., Seattle, WA (1984).

[7] Pinkus, A. R., and Task, H. L., "Quad-emissive Display for Multispectral Sensor Analyses," Proc. SPIE 733650, (2009).

[8] Wikipedia, "Generalized logistic curve," http://en.wikipedia.org/wiki/Generalised_logistic_curve, (2010).